Nonlinear Crosswind Diffusion and Discrete Maximum Principle for Stabilized Galerkin Approximations

Erik Burman [a] Alexandre Ern [b]

[a] *DMA, Ecole Polytechnique Fédérale de Lausanne, Switzerland*

[b] *CERMICS, Ecole Nationale des Ponts et Chaussées, 77455 Marne la Vallée cedex 2, France*

Abstract

We investigate nonlinear crosswind diffusion in the framework of stabilized Galerkin approximations of linear and nonlinear model problems. In particular, for linear convection-diffusion problems, we derive rigorously sufficient conditions for a discrete maximum principle to be satisfied. These conditions apply on strictly acute triangulations for linear simplicial finite elements. The new crosswind diffusion operator is compared numerically to other discontinuity capturing schemes which lack theoretical justification. The numerical results are investigated in terms of both solution quality (violation of maximum principle, smearing of internal layers) and computational cost.

Key words: Finite elements, maximum principle, nonlinear diffusion, Petrov-Galerkin method, convection-diffusion, combustion
PACS: 02.70.Dh, 02.60.Cb, 02.60.Lj, 47.11.+j

1 Introduction

The main motivation for this work is the computation of chemically reacting flows using stabilized Galerkin methods. The governing equations for such flows consist of the compressible Navier-Stokes equations coupled with a system of convection-diffusion-reaction equations for the thermochemistry. Usually the flow is convection dominated with very sharp internal layers near flame fronts. It is well known that the standard Galerkin method is ill suited for the computation of such flows. In order to get a stable numerical scheme, a least squares perturbation may be added to the standard formulation yielding a Petrov-Galerkin method like the SUPG method or the streamline diffusion

method [1–4]. Such modifications yield high order methods with reasonable stability properties. However, near sharp fronts, small spurious oscillations remain and will so until the local Peclet number is small enough. These overshoots or undershoots, even if they are relatively small, may have a dramatic effect in chemically reacting flows where it is stringent from both a physical and numerical viewpoint to guarantee that all the species concentrations remain positive.

Because of the complexity of chemically reacting flow equations, the methodology of this paper is to focus on a much simpler problem, a linear homogeneous stationary convection-diffusion equation with non homogeneous boundary data. For this model problem, it is well known that a maximum principle holds, i.e. under some assumptions on the data, the solution attains its maximum and minimum on the boundary. We will say that an approximation method for the convection-diffusion equation satisfies a discrete maximum principle (DMP in short) if the above property is transferred to the discrete problem. The DMP is not only important for the physical reasons mentioned above but it has also important consequences concerning L^∞ convergence, pointwise stability estimates, and L^2 uniform convergence when the diffusion coefficient tends to zero [5–7]. For maximum principles applied to general elliptic partial differential equations of second order, we refer to [8].

The approximation of the convection-diffusion equation in the framework of stabilized Galerkin methods has already been studied extensively in the literature. As a remedy for the presence of overshoots or undershoots near sharp layers, various crosswind diffusion terms have been proposed, either linear [4,7] or nonlinear [2,3,9–11]. Although extensive numerical experimentation has been reported on a wide range of crosswind diffusion operators, a DMP for stabilized Galerkin methods has only been rigorously established when the crosswind dissipation is an order one perturbation [12,10]. In this case, an approximation method with a first order isotropic viscosity is recovered. Thus, *establishing a DMP for* high order *stabilized Galerkin methods is still an open problem.* To this purpose, it seems reasonable to consider nonlinear crosswind diffusion. Indeed, in the framework of unsteady problems, Godunov's theorem establishes that a *linear*, monotonicity preserving method is at most first order accurate [13, p. 177].

The goal of this paper is to study a certain class of methods based on nonlinear crosswind diffusion for the convection-diffusion equation and to derive sufficient conditions that will guarantee a DMP. These conditions apply to linear simplicial elements on strictly acute triangulations. More specifically, upon writing the finite element residual as a sum over the neighboring elements, we prove that it is possible to choose the nonlinear crosswind diffusion operator in such a way that all the terms have the same sign if the discrete solution presents locally a minimum or a maximum. Using this technique

of proof for linear problems, one recovers the classical requirement that the stiffness matrix be diagonally dominant with negative off-diagonal entries [5]. For Poisson type problems, this latter property holds for instance when using strictly acute meshes. The acute type condition on the mesh, however, may be weakened as pointed out for instance in [14] and more recently in [15] for tetrahedral triangulations, but these aspects will not be further investigated here in the framework of nonlinear problems.

In the next section, we provide a brief background on stabilized Galerkin methods and the DMP. In section three we present our theoretical results. Finally, in section four, we present numerical results for various linear and nonlinear crosswind diffusion operators. We consider two model problems : a linear convection-diffusion equation and a nonlinear Bunsen flame. We investigate violation of the maximum principle, smearing of internal layers and numerical cost.

2 Stabilized Galerkin methods and the DMP

Let Ω be an open bounded connected subset of $\mathbb{R}^d$ with a Lipschitz boundary $\partial\Omega$. We consider the two-dimensional homogeneous convection-diffusion equation

$$-\varepsilon\Delta u + \beta\cdot\nabla u = 0 \quad \text{in } \Omega, \tag{1}$$

$$u = g \quad \text{on } \partial\Omega, \tag{2}$$

where $\beta \in L^\infty(\Omega)^d$ is a given flow velocity field, ε a diffusion coefficient and g is given in $H^{1/2}(\partial\Omega)$. We assume that β is solenoidal, i.e. $\nabla\cdot\beta = 0$ and that $\varepsilon > 0$ so that the above problem is well posed.

Hereafter, we will use the notation $e_\beta = \frac{\beta}{|\beta|}$ where $|\cdot|$ is the Euclidean norm. For any function v, we denote its *streamline derivative* by $v_\beta = e_\beta\cdot\nabla v$ so that $\beta\cdot\nabla v = |\beta| v_\beta$. Moreover, letting $P_{\beta^\perp} = \mathbf{I} - \frac{\beta\otimes\beta}{|\beta|^2}$ be the orthogonal projector onto the hyperplane $\beta^\perp$ along the line $\mathbb{R}\beta$, we denote the *crosswind derivative* of any function v by $v_{\beta^\perp} = P_\beta\cdot\nabla v$.

Let $\mathcal{T}$ be a triangulation of Ω with no overlapping nodes. For any simplex $K \in \mathcal{T}$, we denote h_K its diameter, m_K its measure and we set $h = \max_{K\in\mathcal{T}} h_K$. For a function $v \in L^\infty(\Omega)^m$ $(m \geq 1)$, $|v|_K$ denotes the $L^\infty(K)^m$ norm of its restriction to K.

Let V_h^g and V_h^0 be the finite element spaces defined by

$$V_h^g = \{v \in C^0(\bar\Omega);\, v_{|K} \in P_1(K), \forall K \in \mathcal{T}; v = \mathcal{P}g \text{ on } \partial\Omega\},$$

$$V_h^0 = \{v \in C^0(\bar{\Omega});\, v_{|K} \in P_1(K), \forall K \in \mathcal{T}; v = 0 \text{ on } \partial\Omega\},$$

where $\mathcal{P}$ denotes the L^2-projection onto the space of piecewise affine functions on the boundary. We may then formulate the streamline diffusion method for (1)-(2) as follows: find $U \in V_h^g$ such that

$$a_{sd}(U, v) = 0, \quad \forall v \in V_h^0,$$

where the bilinear form $a_{sd}(U, v)$ is given by

$$a_{sd}(U, v) = (\varepsilon \nabla U, \nabla v) + (|\beta| U_\beta, v) + (\eta U_\beta, v_\beta). \tag{3}$$

Here, $(\cdot, \cdot)$ denotes the $L^2(\Omega)$ inner product. The streamline diffusion coefficient η is constant elementwise with η_K proportional to $|\beta|_K h_K$. The linear system (3) has positive definite symmetric part and the discrete solution U is unique.

It is well known that the streamline diffusion method is accurate but produces unacceptable oscillations near sharp layers. As a remedy, an additional crosswind diffusion term, often called *shock capturing term* or *discontinuity capturing term* may be added in the form

$$b_{cd}(U; v) = (\eta f(U) U_{\beta^\perp}, v_{\beta^\perp}) = (\eta f(U) \nabla U, P_\beta \cdot \nabla v)$$

where $f(U)$ is some function of the finite element solution U. The streamline-crosswind diffusion method may then be formulated as follows: find $U \in V_h^g$ such that

$$a_{sd}(U, v) + b_{cd}(U; v) = 0, \quad \forall v \in V_h^0. \tag{4}$$

Note that $f(U)$ represents the relative amount of crosswind diffusion introduced in the method with respect to the streamline diffusion. With $f = 0$ we recover the usual streamline diffusion method while the choice $f = 1$ yields a first order method with isotropic diffusion of order h.

The question addressed in this paper is how to chose $f(U)$ so that a DMP can be rigorously proven for (4) while retaining high accuracy. For the model problem (1)-(2), the DMP is formulated as follows:

$$\forall x \in \Omega, \quad \min_{y \in \partial\Omega} g(y) \leq U(x) \leq \max_{y \in \partial\Omega} g(y).$$

When the triangulation is strictly acute, it was proven in [10] that upon taking

$$\eta_K = c_K \frac{|\beta|_K h_K}{2} \qquad \text{and} \qquad f = 1, \tag{5}$$

where c_K is a certain function of the angles of K, the method (4) satisfies the DMP. Thus unphysical oscillations are fully wiped out, but at the price of accuracy since the method is only first order.

Different choices of $f(U)$ preserving accuracy have been proposed in the literature. They may be split into two broad categories. In the first one, the function f does not depend on U so that the discrete system retains the linear features of the model problem. Furthermore, ηf is usually of order $3/2$ with respect to h in order to preserve accuracy. For instance, the choice

$$\eta f = \max(h^{3/2} - \varepsilon, 0),$$

was introduced by Johnson et al. [16,4] and generalized by Lube [17]. In a more recent contribution, Shih and Elman [7] consider

$$\eta f = \eta_{cd} h^{3/2} \tag{6}$$

and the stabilization parameters η and η_{cd} are chosen in such a way as to give uniform convergence in ε.

In the second category, $f(U)$ depends on U so that the discrete system is nonlinear regardless of the model problem. In the flame problems we are eventually interested in, this is not a severe penalty since one has already to cope with highly nonlinear source terms for the thermochemistry. The most recent $f(U)$ in this category is the one suggested by Codina [10] and given by

$$f(U) = \frac{|\mathbf{r}(U)|}{|\beta|\,|\nabla U|}, \tag{7}$$

where $\mathbf{r}(U)$ is the finite element residual, i.e. the finite element solution inserted in the differential equation. Numerical experiments showed reasonable numerical behavior of the proposed method but there is no guarantee for a DMP.

In the following, we shall restrict ourselves to the case where the velocity field β is constant elementwise and consider a particular form of crosswind diffusion where $f(U)$ only depends on the angle between $\nabla U|_K$ and $\beta|_K$. Upon denoting by θ_K this angle, the crosswind diffusion term now reads

$$b_{cd}(\theta_K; U, v) = (\eta f(\theta_K) U_{\beta^\perp}, v_{\beta^\perp}). \tag{8}$$

For instance, when using linear simplicial elements, the crosswind diffusion term proposed by Codina takes on the simple form

$$f(\theta_K) = |\cos\theta_K|.$$

The streamline-crosswind diffusion method we shall consider is thus: find $U \in V_h^g$ such that

$$a_{sd}(U, v) + b_{cd}(\theta_K; U, v) = 0, \quad \forall v \in V_h^0. \tag{9}$$

In the next section, we will obtain an explicit expression for f such that a DMP holds for (9) on strictly acute meshes.

Remark 2.1 *The formulation (9) can be rewritten in a Petrov-Galerkin form*

$$(\varepsilon\nabla U, \nabla v) + (\beta\cdot\nabla U, v) + (\eta'\beta\cdot\nabla U, \widetilde{\beta}\cdot\nabla v) = 0, \quad \forall v\in V_h^0,$$

where η' is a renormalized streamline diffusion coefficient given elementwise by $\eta'_K = \frac{\eta_K}{|\beta|_K^2}$ and

$$\widetilde{\beta} = \beta + f(\theta_K)(\tan\theta_K)\beta_1^{\perp}.$$

The vector $\beta_1^{\perp}$ is given by the rotation of β with angle $+\frac{\pi}{2}$ in the plane spanned by ∇U and β. The above expression results from $(U_{\beta^\perp}, v_{\beta^\perp}) = \frac{1}{|\beta|^2}(\beta_1^{\perp}\cdot\nabla U, \beta_1^{\perp}\cdot\nabla v)$ and $\beta_1^{\perp}\cdot\nabla U = \tan\theta_K|\beta|U_\beta$. As a result, (9) may also be viewed as a Galerkin/least squares formulation with a modified advection direction for the stabilization term.

3 Main results

In this section, we first present some preliminary results on strictly acute triangulations, then obtain sufficient conditions for the DMP with first order isotropic viscosity and finally prove the main results for the nonlinear formulation.

3.1 Strictly acute triangulations and preliminary results

On a given simplex $K\in\mathcal{T}$, we denote by $(\psi_0^K,\ldots,\psi_d^K)$ the local shape functions (also termed nodal functions or barycentric coordinates) and set $e_i = \frac{\nabla\psi_i^K}{|\nabla\psi_i^K|}$ for $0\le i\le d$. Hereafter we shall assume that the triangulation $\mathcal{T}$ is *strictly acute* in the following sense:

$$\forall K\in\mathcal{T},\ \exists\alpha_K>0, \quad \max_{0\le i<j\le d}\frac{(\psi_i^K,\psi_j^K)}{|\psi_i^K|\,|\psi_j^K|}\le -\sin\alpha_K.$$

In two space dimensions, α_K is simply given by $\frac{\pi}{2}$ minus the largest angle of the triangle K while in three space dimensions one has to consider the largest angle among the six pairs of faces of the tetrahedron.

Lemma 3.1 *Let $\mathcal{T}$ be a strictly acute triangulation, $U\in V_h^g$ and $K\in\mathcal{T}$. Let i_0 be the vertex number where U is minimal on K, set $\nabla U_{||}^K = (\nabla U|_K\cdot e_{i_0})e_{i_0}$*

and $\nabla U_\perp^K = \nabla U|_K - \nabla U_\parallel^K$. *Then we have*

$$|\nabla U_\parallel^K| \geq \tan\alpha_K \, |\nabla U_\perp^K|. \tag{10}$$

In addition, the same result holds for the vertex where U *is maximal on* K.

Proof Without loss of generality, we assume that U is minimal on K at the vertex $i_0 = 0$. Introduce the Gram matrix $G_{ij} = (e_i, e_j)$, $0 \leq i, j \leq d$, and the quantities $\delta_i = U_i - U_0 \geq 0$ for $1 \leq i \leq d$. We may then write $\nabla U|_K = \sum_{i=1}^d \delta_i e_i$, $\nabla U_\parallel^K = (\sum_{i=1}^d \delta_i G_{0i}) e_0$ and $\nabla U_\perp^K = \sum_{i=1}^d \delta_i (e_i - G_{0i} e_0)$. A straightforward calculation then yields

$$|\nabla U_\parallel^K|^2 = \sum_{i=1}^d \delta_i^2 G_{0i}^2 + 2 \sum_{i<j} \delta_i \delta_j G_{0i} G_{0j},$$

and

$$|\nabla U_\perp^K|^2 = \sum_{i=1}^d \delta_i^2 (1 - G_{0i}^2) + 2 \sum_{i<j} \delta_i \delta_j (G_{ij} - G_{0i} G_{0j}).$$

Since the triangulation is strictly acute, we have $G_{0i}^2 \geq (\tan\alpha_K)^2 (1 - G_{0i}^2)$. Moreover, the last term in the expression for $|\nabla U_\parallel^K|^2$ is positive whereas it is negative for $|\nabla U_\perp^K|^2$. The estimate (10) is then easily obtained. □

Corollary 3.2 *Keep the assumptions and notation of lemma 3.1. Assume further that* $\nabla U|_K \neq 0$ *and denote by* ω_{K,i_0} *the angle between* $\nabla U|_K$ *and* e_{i_0}. *If* i_0 *corresponds to a minimum, we have*

$$\frac{\pi}{2} + \alpha_K \leq \omega_{K,i_0} \leq \frac{3\pi}{2} - \alpha_K, \tag{11}$$

and correspondingly in the case of a maximum

$$-\frac{\pi}{2} + \alpha_K \leq \omega_{K,i_0} \leq \frac{\pi}{2} - \alpha_K, \tag{12}$$

Proof Direct consequence of lemma 3.1. □

3.2 DMP for first order isotropic viscosity

We present here sufficient conditions for the DMP to hold in the case of first order isotropic viscosity. The result is analogous to the one obtained in [10] but the technique of proof is slightly different.

Proposition 3.3 *Let $\mathcal{T}$ be a strictly acute triangulation. For $K \in \mathcal{T}$, let $\gamma_K = \frac{|\beta|_K h_K}{2\varepsilon}$ be the local Peclet number, set $\sigma_K = h_K \min_{0\le i\le d} |\nabla \psi_i^K|$ and let c_K be such that*

$$\forall K \in \mathcal{T}, \quad c_K \geq \frac{2}{(d+1)\ \sigma_K \sin\alpha_K} - \frac{1}{\gamma_K}. \tag{13}$$

Then the formulation (9) with

$$\eta_K = c_K \frac{|\beta|_K\, h_K}{2} \qquad \text{and} \qquad f = 1, \tag{14}$$

satisfies the DMP.

Proof For a given vertex S_0 in the triangulation, we denote by $V(S_0)$ the set of elements K in $\mathcal{T}$ sharing this vertex. Assume that U reaches its minimum on the vertex S_0 and that $S_0 \in \Omega$. Let $v_0 \in V_h^0$ be the global shape function associated with vertex S_0 (i.e. $v_0(S_0) = 1$ and v_0 vanishes at all the other vertices of $\mathcal{T}$). Denote by ω_K the angle between $\nabla U|_K$ and ∇v_0 on K. Then, testing (9) with $v = v_0$ yields

$$\sum_{K\in V(S_0)} B_K \left(\frac{1}{d+1} \cos\theta_K + (C_K + D_K)\cos\omega_K \right) = 0, \tag{15}$$

where $B_K = \mathrm{m}_K\, |\beta|_K\, |\nabla U|_K$, $C_K = \frac{\eta\,|\nabla v_0|}{|\beta|_K}$ and $D_K = \frac{\varepsilon\,|\nabla v_0|}{|\beta|_K}$. From corollary 3.2, we deduce that $\cos\omega_K \leq -\sin\alpha_K$. We thus have

$$\begin{aligned}
(C_K + D_K)\cos\omega_K &\leq -\sin\alpha_K (C_K + D_K) \\
&\leq -\sin\alpha_K \tfrac{h_K |\nabla v_0|}{2} (c_K + \tfrac{1}{\gamma_K}) \\
&\leq -\sin\alpha_K \tfrac{\sigma_K}{2} (c_K + \tfrac{1}{\gamma_K}),
\end{aligned}$$

and we readily see using (13) that all the terms in the sum (15) are negative. Hence they all vanish, which implies that $\nabla U|_K = 0$ for all $K \in V(S_0)$. We then easily deduce that U can only reach its minimum at the boundary. The proof for the case of a maximum is similar. □

Remark 3.4 *The constant c_K in (13) explodes as $\alpha_K \to 0^+$.*

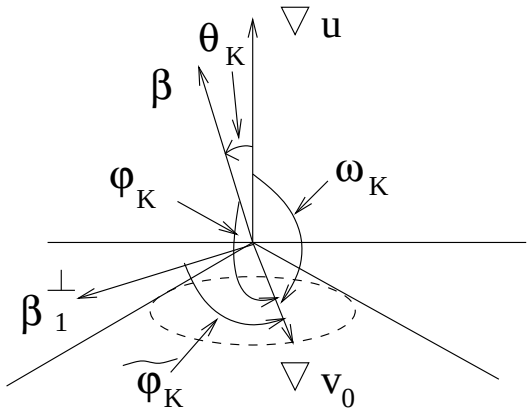

Fig. 1. The various angles considered in the proof of theorem 3.5.

3.3 DMP for nonlinear crosswind diffusion

Theorem 3.5 *Let $\mathcal{T}$ be a strictly acute triangulation. For $K \in \mathcal{T}$, let γ_K and σ_K be defined as in proposition 3.3, let c_K be such that*

$$\forall K \in \mathcal{T}, \quad c_K \geq \frac{2}{(d+1)\sigma_K \sin \alpha_K},$$

and set $\widetilde{\gamma}_K = c_K \gamma_K$. Then the formulation (9) with

$$\eta_K = c_K \frac{|\beta|_K \, h_K}{2},$$

and

$$f(\theta_K) = \max\left(\frac{1 + \tan\alpha_K \tan(\tilde{\theta}_K/2)}{1 + \tan\alpha_K \tan\tilde{\theta}_K} - \frac{1}{\widetilde{\gamma}_K} \frac{\sin\alpha_K}{\cos(\tilde{\theta}_K - \alpha_K)\sin\tilde{\theta}_K}, 0 \right), \quad (16)$$

with $\tilde{\theta}_K = \min(\widehat{\theta}_K, \pi - \widehat{\theta}_K)$ and $\widehat{\theta}_K = \theta_K \bmod \pi$ satisfies the DMP.

Proof (i) Let S_0 be a vertex of $\mathcal{T}$ in Ω and v_0 the corresponding global shape function. Recalling that $\beta_1^\perp$ is given by the rotation of β with angle $+\frac{\pi}{2}$ in the plane spanned by ∇U and β, we denote by ω_K the angle between $\nabla U|_K$ and ∇v_0, by φ_K the angle between β and ∇v_0 and by $\widetilde{\varphi}_K$ the angle between $\beta_1^\perp$ and ∇v_0 (see figure 1). We may then write

$$\begin{aligned} \cos\varphi_K &= \cos\theta_K \cos\omega_K + \sin\theta_K \sin\omega_K \cos\xi \\ \cos\widetilde{\varphi}_K &= -\sin\theta_K \cos\omega_K + \cos\theta_K \sin\omega_K \cos\xi \end{aligned}$$

for a certain $\xi \in [0, 2\pi]$ and thus

$$\cos\omega_K = \cos\theta_K \cos\varphi_K - \sin\theta_K \cos\widetilde{\varphi}_K.$$

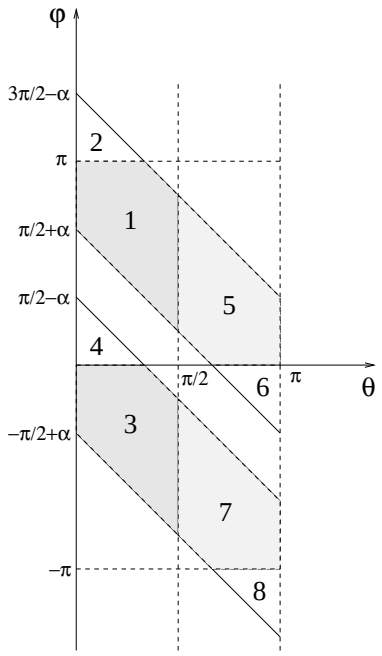

Fig. 2. The different domains in the (θ_K, φ_K) plane for potential overshoot or undershoot (diagonal lines have slope -1).

Using the above notation, (9) may be cast into the form

$$\sum_{K\in V(S_0)} B'_K \left(\tau_K \sin\alpha_K \cos\theta_K \ + \left(1+\tfrac{1}{\widetilde{\gamma}_K}\right)\cos\theta_K \cos\varphi_K \right. \\ \left. - \left(f+\tfrac{1}{\widetilde{\gamma}_K}\right)\sin\theta_K \cos\widetilde{\varphi}_K\right) = 0, \tag{17}$$

with $B'_K = \mathrm{m}_K\, \eta_K\, |\nabla U|_K\, |\nabla v_0|_K$ and $\tau_K = \frac{\sigma_K}{h_K |\nabla v_0|_K} \leq 1$. In particular, in the 2D case we simply have $\cos\widetilde{\varphi}_K = \sin\varphi_K$ and (17) reads

$$\sum_{K\in V(S_0)} B'_K \Big(\tau_K \sin\alpha_K \cos\theta_K + \mathcal{F}(\theta_K, \varphi_K)\Big) = 0,$$

with

$$\mathcal{F}(\theta_K, \varphi_K) = \left(1+\frac{1}{\widetilde{\gamma}_K}\right)\cos\theta_K \cos\varphi_K - \left(f+\frac{1}{\widetilde{\gamma}_K}\right)\sin\theta_K \sin\varphi_K.$$

(ii) We now study some properties of the functional $\mathcal{F}(\theta_K, \varphi_K)$ with the nonlinear crosswind diffusion f chosen as in (16). Consider the domains D_1 to D_4 in the (θ_K, φ_K) plane as illustrated on figure 2. Let us show that if (θ_K, φ_K) lies in $D_1 \cup D_2$, we have

$$\pm\tau_K \sin\alpha_K \cos\theta_K + \mathcal{F}(\theta_K, \varphi_K) \leq 0, \tag{18}$$

whereas if (θ_K, φ_K) lies in $D_3 \cup D_4$, we have

$$\pm\tau_K \sin\alpha_K \cos\theta_K + \mathcal{F}(\theta_K, \varphi_K) \geq 0. \tag{19}$$

Assume first that $(\theta_K, \varphi_K) \in D_1$. Since $\sin\theta_K \sin\varphi_K \geq 0$ and $\cos\theta_K \geq 0$, a sufficient condition for (18) to hold is that $f + \frac{1}{\widetilde{\gamma}_K} \geq \psi(\varphi_K)\cot\theta_K$ with

$$\psi(\varphi_K) = \frac{\sin\alpha_K}{\sin\varphi_K} + \left(1 + \frac{1}{\widetilde{\gamma}_K}\right)\cot\varphi_K.$$

Since the function ψ is decreasing, a sufficient condition for (18) to hold is that

$$f + \frac{1}{\widetilde{\gamma}_K} \geq \psi\left(\frac{\pi}{2} + \alpha_K - \theta_K\right)\cot\theta_K,$$

and a straightforward calculation yields

$$f \geq \frac{1 + \tan\alpha_K \tan(\theta_K/2)}{1 + \tan\alpha_K \tan\theta_K} - \frac{1}{\widetilde{\gamma}_K}\frac{\sin\alpha_K}{\cos(\theta_K - \alpha_K)\sin\theta_K}.$$

Thus the choice (16) guarantees (18). Assume next that $(\theta_K, \varphi_K) \in D_2$. Then a straightforward calculation shows that in order to guarantee (18), it suffices to have $f \leq 1$. Indeed, in such case, we get

$$\begin{aligned}
\pm\tau_K \sin\alpha_K \cos\theta_K + \mathcal{F}(\theta_K, \varphi_K) &\leq \pm\tau_K \sin\alpha_K \cos\theta_K + \left(1 + \tfrac{1}{\widetilde{\gamma}_K}\right)\cos(\theta_K + \varphi_K) \\
&\leq \pm\tau_K \sin\alpha_K \cos\theta_K - \left(1 + \tfrac{1}{\widetilde{\gamma}_K}\right)\sin\alpha_K \\
&\leq 0.
\end{aligned}$$

Moreover $f \leq 1$ trivially results from (16) so that inequality (18) is also established for $(\theta_K, \varphi_K) \in D_2$. The proof of (19) when (θ_K, φ_K) lies in $D_3 \cup D_4$ is similar and is omitted for brevity.
(iii) Consider now $\theta_K \in [\frac{\pi}{2}, \pi]$ and the domains D_5 to D_8 illustrated in figure 2. It is readily seen that domains D_5 to D_8 are recovered from D_1 to D_4 using the symmetry $\theta_K \to \pi - \theta_K$ and $\varphi_K \to -\varphi_K$. Since $\mathcal{F}(\theta_K, \varphi_K)$ changes sign under such symmetry, we deduce that if (θ_K, φ_K) lies in $D_5 \cup D_6$, we have

$$\pm\tau_K \sin\alpha_K \cos\theta_K + \mathcal{F}(\theta_K, \varphi_K) \leq 0,$$

whereas if (θ_K, φ_K) lies in $D_7 \cup D_8$, we have

$$\pm\tau_K \sin\alpha_K \cos\theta_K + \mathcal{F}(\theta_K, \varphi_K) \geq 0.$$

Moreover, if $\theta_K \in [\pi, 2\pi]$, we consider the translation $\theta_K \to \theta_K - \pi$ and $\varphi_K \to \varphi_K - \pi$ which leaves $\mathcal{F}(\theta_K, \varphi_K)$ invariant. To sum up, we have proven that for all $\theta_K \in [0, 2\pi]$, letting $\widehat{\theta}_K = \theta_K \bmod \pi$, we have

$$(\widehat{\theta}_K, \varphi_K) \in D_1 \cup D_2 \cup D_5 \cup D_6 \Longrightarrow \pm\tau_K \sin\alpha_K \cos\theta_K + \mathcal{F}(\theta_K, \varphi_K) \leq 0,$$

and

$$(\widehat{\theta}_K, \varphi_K) \in D_3 \cup D_4 \cup D_7 \cup D_8 \Longrightarrow \pm\tau_K \sin\alpha_K \cos\theta_K + \mathcal{F}(\theta_K, \varphi_K) \geq 0.$$

(iv) DMP in the 2D case. Assume that U reaches its minimum on vertex S_0. We then deduce from corollary 3.2 that for all $K \in V(S_0)$, the pairs $(\widehat{\theta}_K, \varphi_K)$ lie in $D_1 \cup D_2 \cup D_5 \cup D_6$. Therefore, from the above inequalities, we deduce that all the elements $K \in V(S_0)$ yield a negative contribution to the sum (17). Thus the discrete solution U is necessarily constant on $V(S_0)$ and from this property it readily follows that $\min_{y\in\Omega} U(y) \geq \min_{y\in\partial\Omega} g(y)$. The case where U reaches its maximum on vertex S_0 is treated similarly.
(v) DMP for arbitrary space dimension. We notice that (17) can be recast into the form

$$\sum_{K\in V(S_0)} B'_K \left(\tau_K \sin\alpha_K \cos\theta_K \ + \left(1 + \tfrac{1}{\widetilde{\gamma}_K}\right) \cos\omega_K \right.$$
$$\left. - (f-1) \sin\theta_K \cos\widetilde{\varphi}_K\right) = 0,$$

which we rewrite for convenience as

$$\sum_{K\in V(S_0)} B'_K\Big(a_K + b_K + c_K(\xi)\Big) = 0,$$

where the angle ξ has been introduced in part (i) of the proof. Recalling the expression for $\cos\widetilde{\varphi}_K$, it is readily seen that $c_K(\xi)$ takes its extreme values for $\xi = 0 \bmod \pi$ in which case ∇v_0 lies in the plane spanned by ∇U and β so that a 2D situation is recovered. Assume now that U reaches its minimum on vertex S_0. Since

$$a_K + b_K + c_K(\xi) \leq a_K + b_K + \max\Big(c(0), c(\pi)\Big),$$

we deduce from the 2D case that $a_K + b_K + c_K(\xi) \leq 0$. Thus all the elements $K \in V(S_0)$ yield a negative contribution to the sum and the proof is completed as before. The case of a maximum is treated similarly by noticing that

$$a_K + b_K + c_K(\xi) \geq a_K + b_K + \min\Big(c(0), c(\pi)\Big) \geq 0,$$

thanks to the 2D case. □

Remark 3.6 *A straightforward calculation shows that the nonlinear cross-*

wind diffusion operator given by (16) may be equivalently recast into the form

$$f(\theta_K) = \max\left(\frac{1+\tan\alpha_K\sqrt{\frac{1-|\cos\theta_K|}{1+|\cos\theta_K|}}}{1+\tan\alpha_K|\tan\theta_K|} - \frac{1}{\widetilde{\gamma}_K}\frac{\tan\alpha_K}{|\cos\theta_K\sin\theta_K| + \tan\alpha_K\sin^2\theta_K}, 0\right), \tag{20}$$

the above expression being valid for all $\theta_K \in [0, 2\pi]$.

Corollary 3.7 *Keep the notation and assumptions of theorem 3.5 except for the function* $f(\theta_K)$ *which is now given by*

$$f(\theta_K) = \frac{1+\tan\alpha_K\sqrt{\frac{1-|\cos\theta_K|}{1+|\cos\theta_K|}}}{1+\tan\alpha_K|\tan\theta_K|}, \tag{21}$$

or, equivalently, by

$$f(\theta_K) = \frac{|U_\beta|_K}{(|U_\beta|_K + \tan\alpha_K|U_{\beta^\perp}|_K)}\,\frac{(|U_\beta|_K + |\nabla U|_K + \tan\alpha_K|U_{\beta^\perp}|_K)}{|\nabla U|_K + |U_\beta|_K}. \tag{22}$$

Then the formulation (9) satisfies the DMP.

Proof The equivalence between (21) and (22) simply results from the relations $|U_\beta|_K = |\cos\theta_K|\,|\nabla U|_K$ and $|U_{\beta^\perp}|_K = |\sin\theta_K|\,|\nabla U|_K$ thanks to some little algebra. On the other hand, the DMP is a direct consequence of the proof of theorem 3.5. □

Remark 3.8 *Notice that the function* $f(\theta_K)$ *given by either (16) or (21) is lower than one. Thus the amount of crosswind diffusion is always lower than that of streamline diffusion. In addition, (16) yields a lower amount of crosswind diffusion with respect to (21) since it takes into account the physical isotropic diffusion through the rescaled Peclet number* $\widetilde{\gamma}_K$.

Remark 3.9 *It is easily seen that* $f(\theta_K) \to 0^+$ *when* $\theta_K \to \frac{\pi}{2}$. *Thus for convection dominated flows, the crosswind diffusion term vanishes when the residual goes to zero. This ensures that the formulation (9) retains an accuracy similar to the original streamline diffusion method.*

In figure 3, we illustrate the function (21) for various values of the parameter α_K. The solid line corresponds to $\alpha_K = 30°$ (the largest possible value for α_K corresponding to an equilateral triangle), the dashed line to $\alpha_K = 10°$ and the dotted line to $\alpha_K = 1°$. Notice how the well at $\theta_K = 90°$ becomes steeper with decreasing α_K.

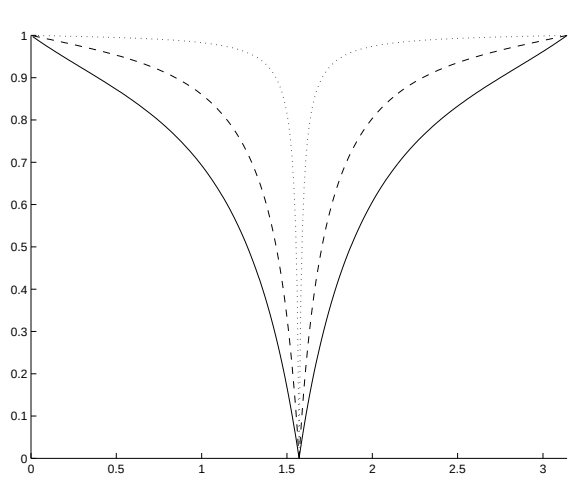

Fig. 3. The nonlinear crosswind diffusion operator (21) as a function of θ_K for different values of α_K; solid line: $\alpha_K = 30°$, dashed line: $\alpha_K = 10°$, dotted line: $\alpha_K = 1°$.

4 Numerical results

In this section we discuss the numerical implementation of the nonlinear crosswind diffusion operator derived from theoretical considerations in the previous section. We consider convection dominated flows where the local Peclet number is small on all practical meshes. The correction due to the coefficient $\widetilde{\gamma}_K$ is not considered and we focus on the nonlinear crosswind diffusion operator (22). Its numerical performance is investigated on various test problems, linear and nonlinear, and compared to that of other methods. The test cases we consider are the solution of (1)-(2) on strictly acute and orthogonal meshes with different flow directions and the computation of a Bunsen flame with simple chemistry.

4.1 Numerical implementation

The discrete problem (9) yields a nonlinear system of equations of the form $F(X) = 0$. A numerical solution is obtained using a damped Newton's method: given an initial guess X^0, a sequence of iterates X^n is generated according to

$$J(X^n)(X^{n+1} - X^n) = -\lambda^n F(X^n), \tag{23}$$

where $J(X^n)$ denotes the Jacobian matrix of the nonlinear residual F at X^n and λ^n the damping parameter. The Jacobian matrix is evaluated numerically using perturbed residual evaluations and the linear system (23) is solved numerically with a Krylov iterative method with an appropriate preconditionner (typically BiCGStab with an ILU preconditionner). Convergence of Newton's method is achieved when the normalized Euclidean norm of the update vector

$X^{n+1} - X^n$ is less than a prescribed tolerance (typically 10^{-5}).

With the crosswind diffusion operator given by (22), Newton's method exhibits poor stability properties and its convergence domain is extremely narrow. Such difficulties stem on the one hand from the presence of absolute values which must be differentiated in the Jacobian matrix and on the other hand from the fact that the angle θ_K is ill defined in the regions where ∇U is very small.

In order to enhance convergence of Newton's method, we introduce in the numerical experiments reported below the following two modifications of the nonlinear crosswind diffusion operator. First we consider a regularized absolute value $|x|_{reg} = x \tanh(\frac{x}{\epsilon_{reg}})$, so that (22) becomes

$$f_1(\theta_K, \epsilon_{reg}) = \frac{|U_\beta|_{reg}}{(|U_\beta|_{reg} + \tan\alpha_K |U_{\beta^\perp}|_{reg})} \frac{(|U_\beta|_{reg} + |\nabla U|_K + \tan\alpha_K |U_{\beta^\perp}|_{reg})}{|\nabla U|_K + |U_\beta|_{reg}}. \tag{24}$$

Since we treat here a 2D case, we have $U_{\beta^\perp} = \beta_1^\perp \cdot \nabla U$ and $|\nabla U|_K = \sqrt{U_\beta^2 + U_{\beta^\perp}^2}$. In addition, we also introduce a cutoff function $c(x) = \exp(-\epsilon_{cut} x^{-2})$ that "turns off" the crosswind diffusion operator when the gradient of the discrete solution is small, so that (24) becomes

$$f_2(\theta_K, \epsilon_{reg}, \epsilon_{cut}) = f_1(\theta_K, \epsilon_{reg})\ c(|\nabla U|_K). \tag{25}$$

The approximate crosswind diffusion operators f_1 and f_2 do not guarantee a DMP. However, from a numerical viewpoint, such modifications of the original crosswind diffusion operator f are attractive because the numerical cost for obtaining a discrete solution is much lower. In addition, in our numerical experiments (see below), we observed only a slight degradation in over/undershoots when using (24) and (25). Notice also that f_1 and f_2 tend to f when ϵ_{reg} and ϵ_{cut} tend to zero so that a DMP is recovered.

4.2 Linear test cases: convection-diffusion problems

We consider the convection-diffusion problem (1)-(2) with diffusion coefficient $\varepsilon = 10^{-5}$ and constant flow velocity of norm $|\beta| = 1$ with two different flow angles. The problem is posed on the unit 2D square. Flow angles and boundary conditions are shown in figure 4. The boundary values on the right edge of the square step from $U = 0$ to $U = 1$ at $y = \frac{4}{5}$. The Dirichlet boundary conditions create an internal layer which is convected across the domain and an outflow layer near the outflow boundary.

For the convection-diffusion problem (1)-(2), the quality of the numerical so-

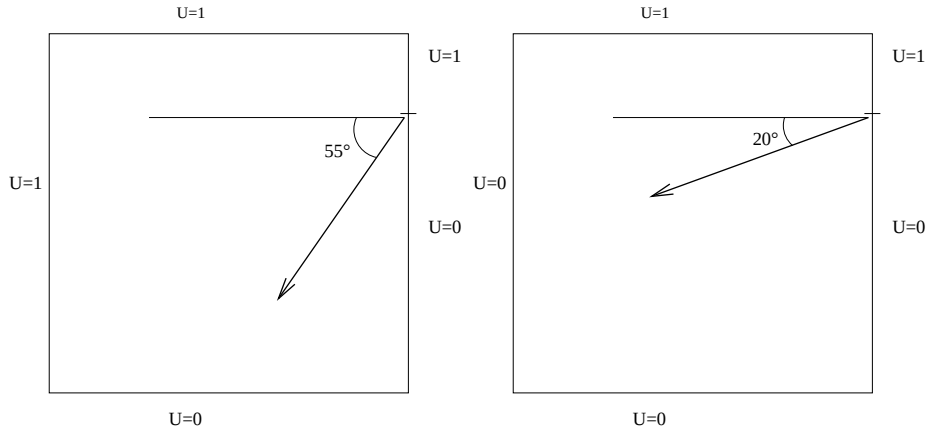

Fig. 4. Flow angle and boundary conditions for test case 1 (left) and 2 (right).

lution will be investigated in terms of layer width and over/undershoots. The layer width Δx will be measured at $y = 0.5$ ($x = 0.5$ for test case two) and is defined as

$$\Delta x = |x_{1\%} - x_{99\%}|$$

where $x_{1\%}$ is the lowest coordinate where $U(x_{1\%}, 0.5) = 0.01\, U_{max}$. Similarly, $x_{99\%}$ is the largest coordinate where $U(x_{99\%}, 0.5) = 0.99\, U_{max}$. Over/undershoots will be measured in percentage of the maximal variation of the solution, $U_{var} = U_{max} - U_{min} = \max_{x\in\partial\Omega} U(x) - \min_{x\in\partial\Omega} U(x)$, according to

$$U_{shoot} = \max(|\max_{x\in\Omega} U(x) - U_{max}|, |\min_{x\in\Omega} U(x) - \min_{x\in\partial\Omega} U(x)|)/U_{var}.$$

Numerical solutions will be obtained on four different strictly acute meshes which are presented in figure 5. The meshes are Delaunay triangulations obtained with the Bowyer-Watson algorithm as described in [18]. On all meshes, the majority of the triangles are close to equilateral. The number of degrees of freedom together with the largest and lowest value for α on each mesh are reported in Table 1.

We first study the impact of the regularization parameter ϵ_{reg} on the behavior of the stabilized method obtained using the approximate crosswind diffusion operator (24). The solution is computed for test case 1 on the second to finest mesh. Solution quality is reported in Table 2 for different values of ϵ_{reg}. For comparison purposes, the last line gives the corresponding results obtained with the standard streamline diffusion method. We notice that even for values as large as $\epsilon_{reg} = 100$, overshoots amount to less than 1%. Furthermore, oscillations decrease significantly when ϵ_{reg} tends to zero. For $\epsilon_{reg} = 10$, the overshoots and undershoots are within the convergence range of Newton's method. Finally, we notice that the value of ϵ_{reg} has only a minor influence on the layer width, lower values of ϵ_{reg} yielding slightly wider layers since they correspond to enhanced numerical diffusion.

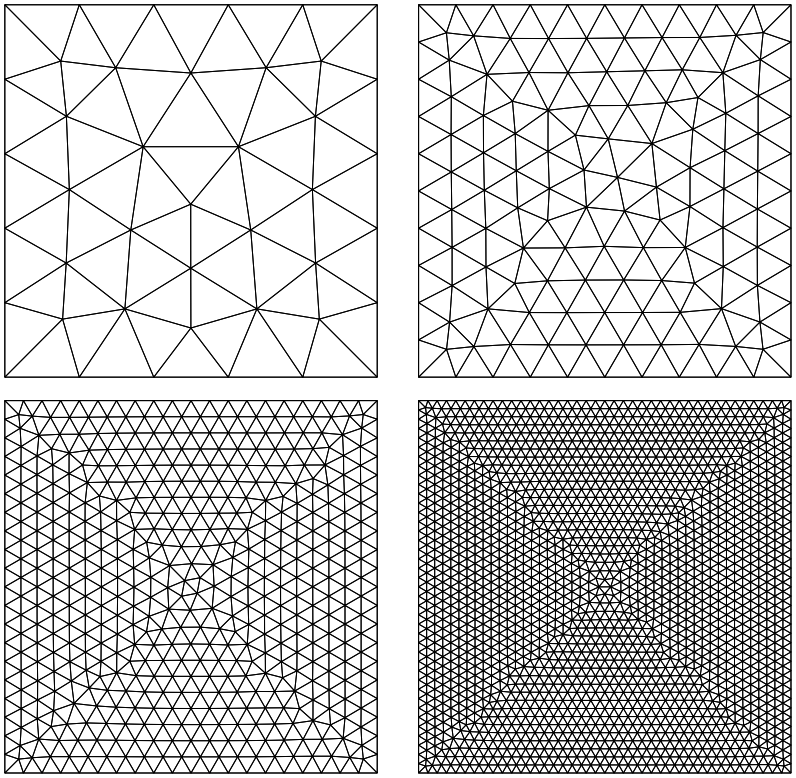

Fig. 5. Delaunay triangulations of strictly acute type used for the convection-diffusion problems.

nodes	min α_K	max α_K
42	6.6	29.5
135	11.7	29.9
503	11.6	30.0
1925	9.9	30.0

Table 1
Number of nodes together with the greatest and lowest value of α_K for the meshes of figure 5.

We next compare six different crosswind diffusion operators, three linear and three nonlinear. We consider

- SD: the standard SD method corresponding to $\eta = \frac{|\beta|h}{2}$ and $f = 0$;
- $O(h)$: $\eta = \frac{|\beta|h}{2}$ and $f = 1$ yielding a first order isotropic viscosity;
- $O(h^{3/2})$: η as before and $f = ch^{1/2}$ $(c = \frac{1}{5})$ corresponding to a shock capturing method with high accuracy;

ϵ_{reg}	overshoot %	undershoot %	layer width
100	0.97	0.003	0.26
50	0.40	0.002	0.26
25	0.03	0.001	0.27
10	0.002	0.0007	0.29
5	0.0002	0.0005	0.32
SD	16.8	3.4	0.36

Table 2
Impact of regularization parameter ϵ_{reg} on solution quality.

- Codina: η as before and $f(U) = c\frac{|U_\beta|}{|\beta||\nabla U|}$ ($c = 0.7$) as suggested by [10];
- f_1: the approximate nonlinear crosswind diffusion operator (24) with $\epsilon_{reg} = 10$;
- f_2: the approximate nonlinear crosswind diffusion operator (25) with $\epsilon_{reg} = 0.8h_K^{-1}$ and $\epsilon_{cut} = 5 \cdot 10^{-4} h_K^{-2}$. Both regularization parameters are taken here in mesh dependent form in order to yield the same order of regularization on all meshes.

Numerical solutions on the finest mesh are shown in figure 6 for test case 1. The $O(h)$ method leads to a dramatic smearing of the internal layer while the $O(h^{3/2})$ method yields a slightly larger layer than the nonlinear methods. Overshoots obtained on the finest mesh are presented in figure 7 while table 3 reports the maximum overshoot observed on each of the four meshes. We notice that our proposed method f_1 together with the linear $O(h)$ method are the only ones that satisfy the DMP, the latter however at the expense of excessive smearing. The linear method of order $O(h^{3/2})$ also performs well with respect to the DMP but the violations tend to increase on the finer meshes, an effect one may also notice in the f_2 case. Finally, we notice that for this test case, Codina's method yields a fair amount of overshoot, indicating that the nonlinear crosswind diffusion which it introduces is not large enough. As a further illustration, we present in figure 8 for the second to finest mesh and a typical numerical solution, a cloud of points obtained as follows. For each element K of the mesh, we plot the point with coordinates θ_K and the minimal amount of crosswind diffusion needed to guarantee a DMP. The solid curve corresponds to the theoretical crosswind diffusion given by (21) while the dotted line corresponds to Codina's method, i.e. $f(\theta_K) = |\cos\theta_K|$. As expected, all the points lie below the solid curve but a fairly large amount of points lies above the dotted curve, indicating potential violation of the DMP.

It is also interesting to assess the numerical cost of the various crosswind diffusion operators. To this purpose, we present in figure 9 the layer width as

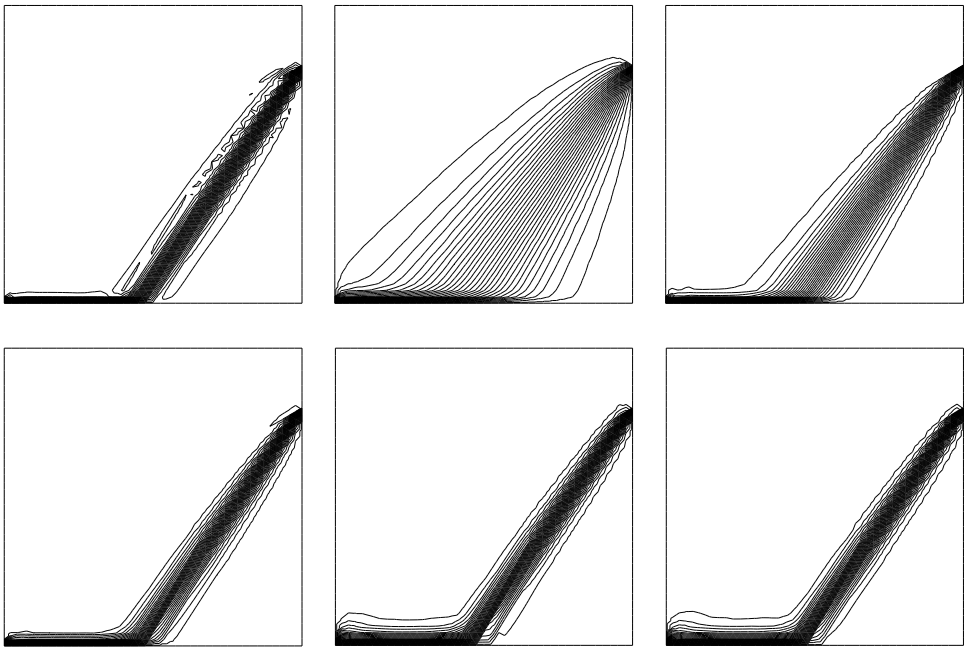

Fig. 6. Numerical solutions obtained with six different crosswind diffusion operators for test case 1 on the finest mesh of figure 5; from left to right and top to bottom: SD, $O(h)$, $O(h^{3/2})$, Codina, f_1, f_2.

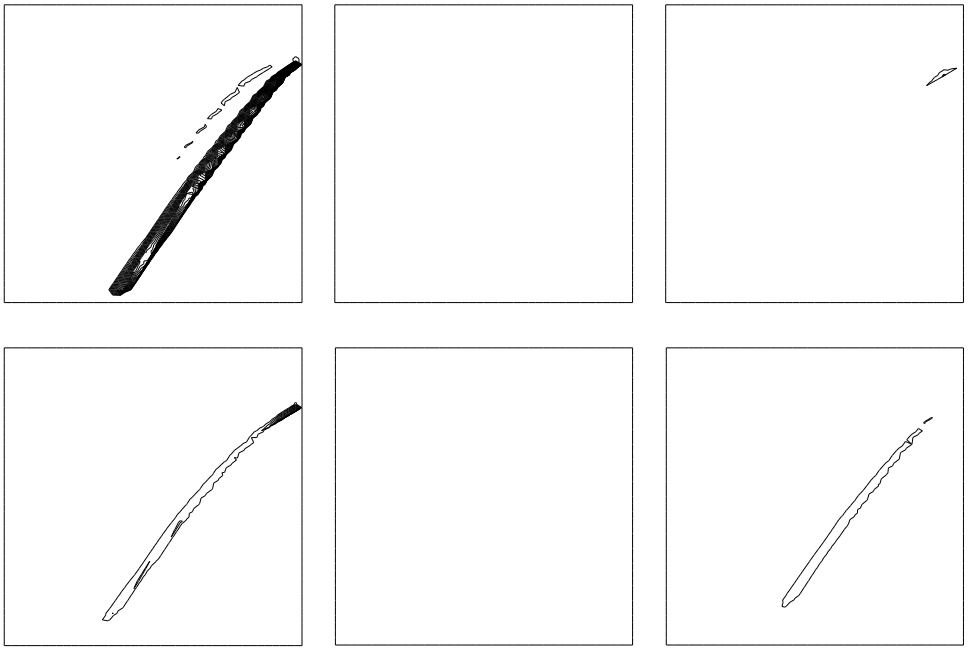

Fig. 7. Overshoots obtained with six different crosswind diffusion operators for test case 1 on the finest mesh of figure 5; from left to right and top to bottom: SD, $O(h)$, $O(h^{3/2})$, Codina, f_1, f_2.

Nodes	SD	$O(h)$	$O(h^{3/2})$	Codina	f_1	f_2
42	16.5	0	0	4.0	0	0
135	17.6	0	0	3.0	0	0.07
503	16.8	0	0	2.4	0	0.48
1925	16.2	0	0.94	2.1	0.03	0.51

Table 3
Maximum overshoot (%) obtained with six different crosswind diffusion operators for test case 1 on the four meshes of figure 5.

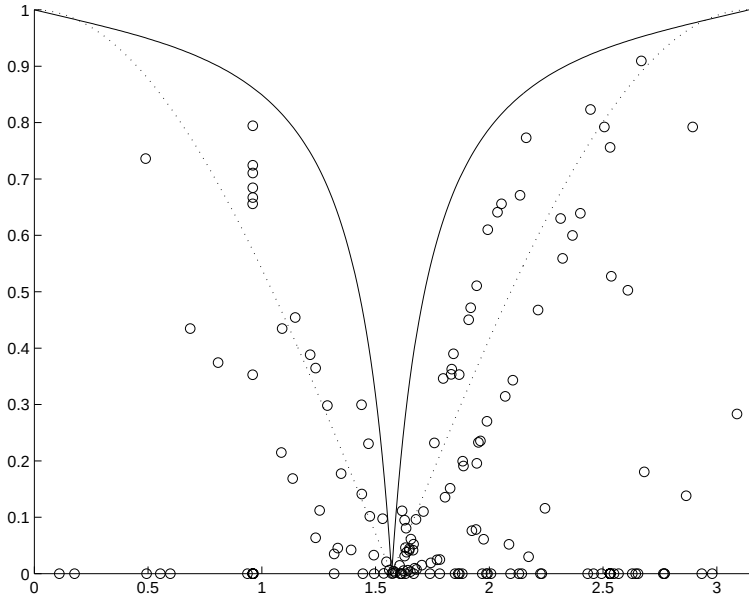

Fig. 8. Comparison of crosswind diffusion operators (21) (solid) and (7) (dotted); all the points must lie below a curve to guarantee a DMP for the corresponding method; points above a curve indicate potential violation of the DMP.

a function of linear algebra cost normalized by the cost associated with the SD method on the finest mesh. On a given mesh, the linear algebra cost is estimated by the total number of BiCGStab iterations in Newton's method multiplied by the square of the number of nodes. For a sharp resolution of the layer width (e.g. 0.2), the method providing the best solution quality, namely f_1, yields a computational cost two orders of magnitude larger than that of the linear, SD method. In this context, the approximate operator f_2 given by (25) appears to offer an attractive compromise between computational cost and solution quality. Indeed, it yields only a minor degradation in terms of overshoots with respect to f_1 while decreasing the computational cost by more than an order of magnitude.

Turning next to test case 2, we report in table 4 the maximum overshoot ob-

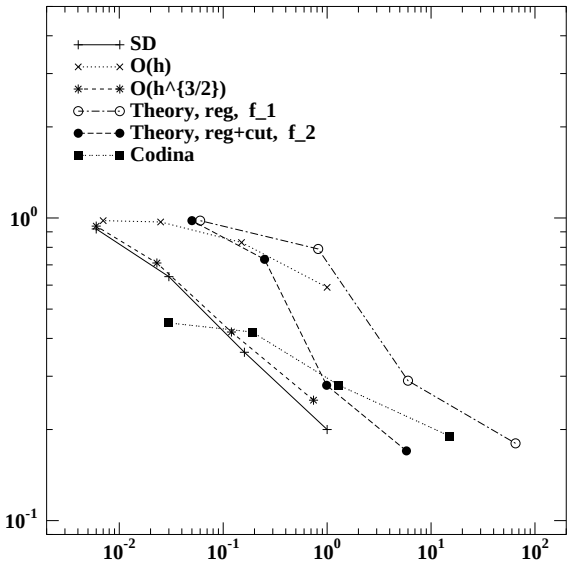

Fig. 9. Layer width as a function of normalized linear algebra cost; test case 1 on strictly acute meshes.

Nodes	SD	$O(h)$	$O(h^{3/2})$	Codina	f_1	f_2
42	13.2	0.00	0.00	2.1	0.00	0.00
135	13.8	0.00	0.00	0.56	1.38	0.27
503	13.5	0.00	0.17	0.39	0.05	0.33
1925	13.7	0.00	1.69	0.48	0.13	0.43

Table 4
Maximum overshoot (%) obtained with six different crosswind diffusion operators for test case 2 on the four meshes of figure 5.

tained on the four meshes of figure 5. The results are similar to those obtained for test case 1. We notice however that the three nonlinear methods now yield overshoots of the same order of magnitude on the finer meshes.

We conclude this section by investigating the performance of the various methods on meshes violating the strictly acute condition. Such meshes are often considered in practice because they are easy to generate since they are often associated with an underlying tensorial mesh. We consider here four meshes obtained by splitting into two triangles the square cells of a tensor product uniform mesh with respectively 5, 10, 20 and 40 nodes per side of the computational domain. For these meshes, $\alpha = 0$ and it is therefore impossible to apply directly the theoretical results of section 3. In our numerical experiments, we set $\alpha_K = \pi/6$ for all triangles when evaluating the approximate

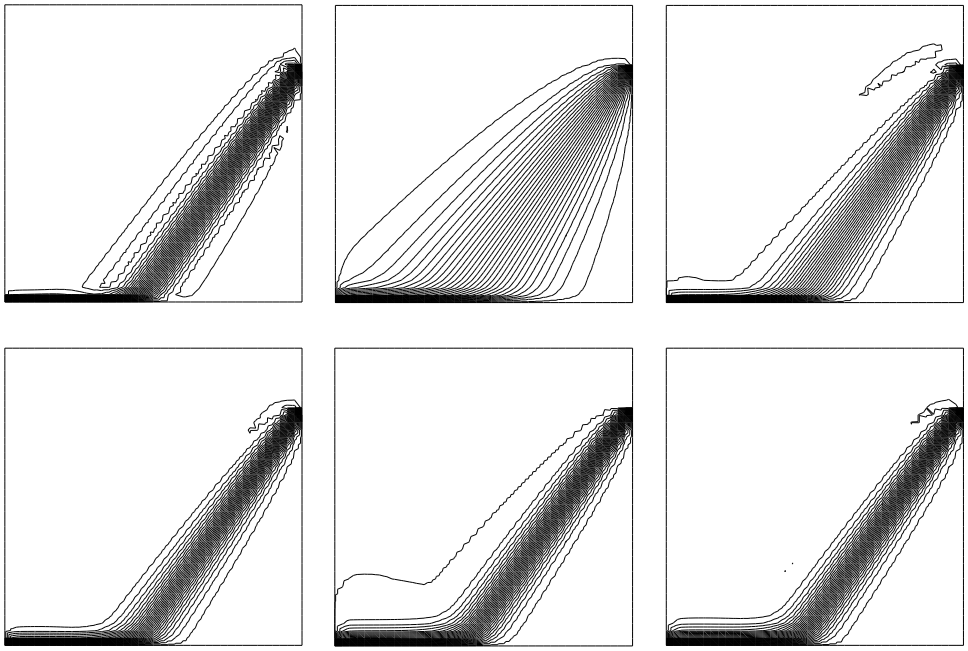

Fig. 10. Numerical solutions obtained with six different crosswind diffusion operators for test case 1 on the finest mesh violating the strictly acute condition; from left to right and top to bottom: SD, $O(h)$, $O(h^{3/2})$, Codina, f_1, f_2.

crosswind diffusion operators (24) and (25). Notice that a lower value for α_K should increase the amount of numerical diffusion. We present results for test case 1, showing the solutions on the finest mesh for the different methods in figure 10 and the location of the overshoots in figure 11. In table 5 we report the maximum overshoots observed on the four meshes. The linear first order method still satisfies the DMP, at the expense however of an excessively smeared internal layer. The performance of the linear $O(h^{3/2})$ method deteriorates substantially on finer meshes, indicating that in some elements the crosswind diffusion has less and less effect. All the nonlinear methods fail to wipe out the overshoots completely. However, the approximate operators f_1 and f_2 yield relatively better results than Codina's. Finally, in order to assess the computational cost of the methods, we present in figure 12 the layer width as a function of linear algebra cost normalized as before. The cost for obtaining a given resolution of the internal layer is comparable for all three nonlinear methods, with f_2 slightly less expensive.

To sum up, our numerical experiments on linear convection-diffusion equations show that among the three nonlinear methods considered, the approximate operator f_2 yields the most attractive compromise between solution quality and computational cost. In the next section, we investigate the numerical performance of the approximate operator f_2 on a strongly nonlinear problem.

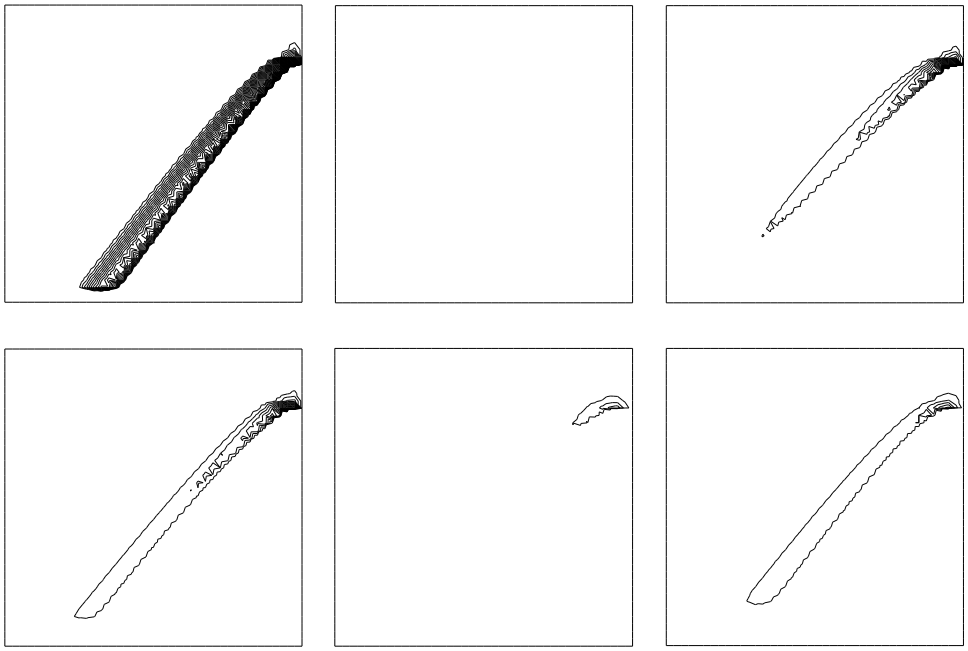

Fig. 11. Overshoots obtained with six different crosswind diffusion operators for test case 1 on the finest mesh violating the strictly acute condition; from left to right and top to bottom: SD, $O(h)$, $O(h^{3/2})$, Codina, f_1, f_2.

Nodes	SD	$O(h)$	$O(h^{3/2})$	Codina	f_1	f_2
36	12.2	0.00	1.3	5.5	1.8	1.5
121	14.3	0.00	4.5	6.5	2.3	2.3
441	14.8	0.00	7.1	6.6	2.1	2.4
1681	14.8	0.00	9.0	6.6	1.7	2.4

Table 5
Maximum overshoot (%) obtained with six different crosswind diffusion operators for test case 1 on four meshes violating the strictly acute condition.

4.3 A nonlinear example: the Bunsen flame

The theory underlying the nonlinear crosswind diffusion operator (22) does not extend to nonlinear problems. A somewhat natural extension of (22) to nonlinear problems is to consider the operator

$$f(U) = \frac{|r(U)|_K}{(|r(U)|_K + \tan\alpha_K |U_{\beta^\perp}|_K)} \, \frac{(|r(U)|_K + |\nabla U|_K + \tan\alpha_K |U_{\beta^\perp}|_K)}{|\nabla U|_K + |r(U)|_K}, \tag{26}$$

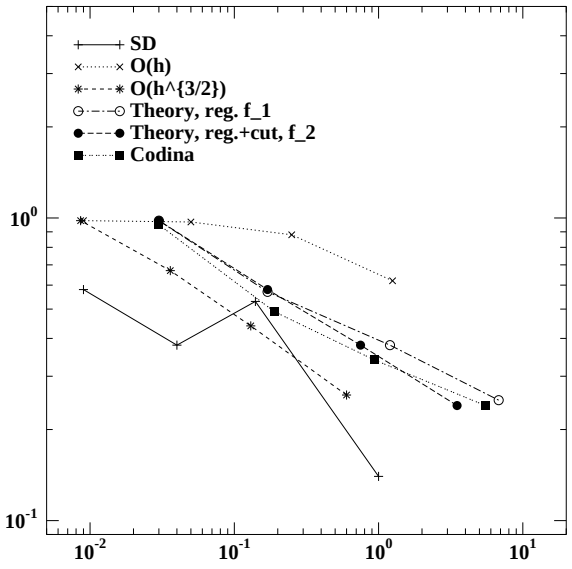

Fig. 12. Layer width as a function of normalized linear algebra cost; test case 1 on meshes violating the strictly acute condition.

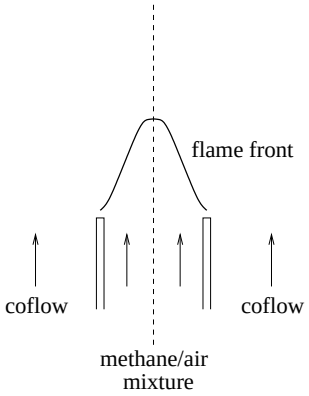

Fig. 13. Schematic of the Bunsen flame configuration.

where $r(U)$ is the nonlinear finite element residual. This expression presents two advantages. First it preserves consistency since $f(U)$ vanishes whenever $r(U) = 0$. Second, for convection dominated flows where $r(U) \simeq U_\beta$, we recover the theoretical expression (22). The operator (26) appears therefore as a reasonable extension to nonlinear problems of the theory developed in the linear case. However, its numerical performance must be carefully assessed.

As an illustration, we consider a methane/air Bunsen flame obtained by flowing a stoichiometric methane/air mixture through a cylindrical tube (see figure 13). The fuel tube has radius 4 mm and the inflow velocity profile is parabolic with a peak velocity of 1.5 m/s. The flame is surrounded by an air coflow with velocity 1 m/s. Reactants and air are flown at room temperature (298 K) so that we expect the temperature to be larger than 298 K throughout the

flame. The governing equations are the compressible Navier-Stokes equations coupled with a system of convection-diffusion-reaction equations for the chemical species and the temperature. We treat a simplified reaction model with four chemical species. Thus, the total number of dependent unknowns is 8: radial and axial velocity components, pressure, temperature and the mass fractions of the 4 chemical species. More details on Bunsen flame modeling may be found for instance in [19].

We compare two numerical methods to approximate the flame problem:

- SD: classical streamline diffusion stabilization. Denoting by ξ a dependent unknown except the pressure, the streamline diffusion coefficient for the corresponding governing equation reads $\eta = \frac{\beta_\xi h}{2}$ where β_ξ is the convection velocity arising in the conservation equation for ξ;
- f_2: streamline diffusion as above plus nonlinear crosswind diffusion for the velocities, temperature and species. For the velocity equations, the crosswind diffusion operator is linear and such that $\eta f = O(h^{3/2})$. For the temperature and species, the nonlinear crosswind diffusion operator (26) is considered with the same regularization of absolute values and cutoff functions as f_2.

The flame governing equations are discretized on a Delaunay triangulation containing about 3300 nodes. Most of the triangles are almost equilateral but a few triangles do not satisfy the strictly acute condition. For practical purposes, the expression (26) is implemented using $\alpha'_K = \max(\alpha_K, 10^\circ)$.

In table 6 we show the main flame charateristics obtained with and without nonlinear crosswind diffusion. The SD method yields an important undershoot in the temperature field thus confirming the need for additional stabilization. The nonlinear crosswind diffusion operator succeeds in removing all the undershoot for temperature. The flame length (resp. width) is however smaller since this quantity decreases (resp. increases) with enhanced diffusion.

A more detailed investigation of the temperature field is presented in figure 14. The temperature undershoot computed by the SD method is quite significant and is due to two combined effects: (i) the convective shear layer between the premixed reactant flow and the air coflow and (ii) the stiff reaction terms arising near the burner lip and at the tip of the flame cone. The temperature undershoot is convected downstream up to the outflow boundary of burnt gases. The nonlinear crosswind diffusion operator handles both phenomena, yielding a numerical solution without undershoot. However, the crosswind stabilized flame is lower and more smeared. We also point out that the convective layer between combustion products and air is resolved in both computations even in the upper part of the domain where the mesh is coarse. This is possible thanks to the nonlinear character of the crosswind operator. Any linear choice

	SD	f_2
Min. temperature (K)	246	298
Max. temperature (K)	2172	2232
Flame length (cm)	0.91	0.69
Flame width (cm)	0.26	0.48
Liftoff (cm)	0.02	0.03

Table 6
Main characteristics of Bunsen flame computed with and without nonlinear crosswind diffusion.

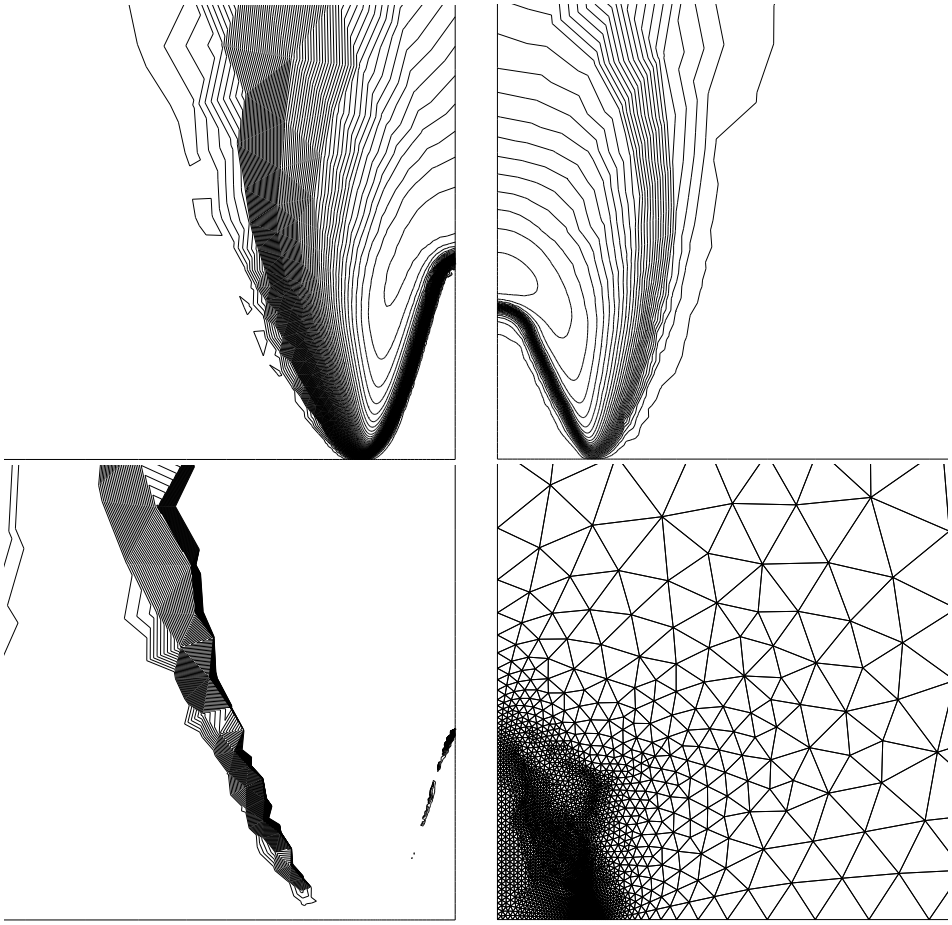

Fig. 14. Top: temperature field as computed without (left) and with nonlinear crosswind diffusion (right); bottom: isotherms in the interval [245,298] computed by the SD method and zoom of the mesh near the burner.

of f would cause excessive smearing of this layer. As a conclusion, for Bunsen flame models, nonlinear crosswind diffusion schemes appear to have a strong influence on solution quality. A more thorough investigation will be presented in a forthcoming paper.

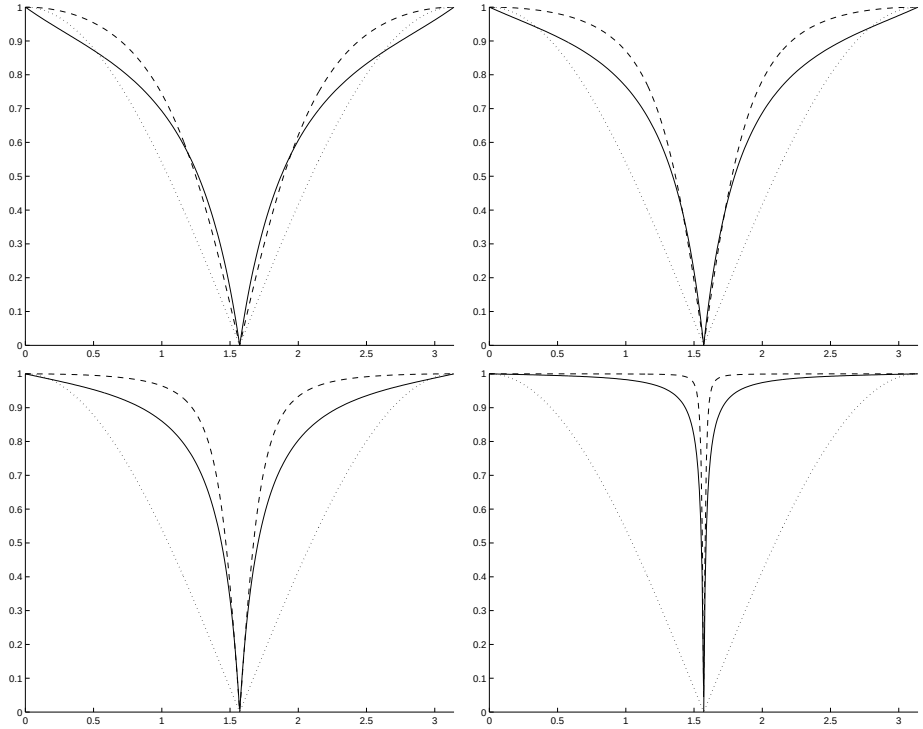

Fig. 15. Comparison of various nonlinear crosswind diffusion operators: solid (21), dashed (27) and dotted (7); from left to right and top to bottom: $\alpha = 30°$, $\alpha = 20°$, $\alpha = 10°$ and $\alpha = 1°$.

Remark 4.1 *Since the theoretical results do not extend to nonlinear problems, other ad hoc modifications of the nonlinear crosswind diffusion operator may be considered, as for instance*

$$f_3(U) = \frac{|\mathbf{r}(U)|}{\sqrt{\mathbf{r}(U)^2 + (\tan\alpha_K \beta^\perp \cdot \nabla U)^2}}. \tag{27}$$

For pure convection problems, this expression coincides with the crosswind diffusion operator suggested by Codina when taking $\alpha = 45°$. In addition, (27) yields a fairly reasonable approximation of the theoretical operator (21) as illustrated in figure 15. A regularized version of f_3 has been implemented for the Bunsen flame problem and appears to produce results similar to those of method f_2.

5 Conclusions

In this paper, we have derived a new nonlinear crosswind diffusion operator which guarantees rigorously the DMP in the case of the linear homogeneous convection-diffusion equation discretized on a strictly acute triangulation with

linear finite elements. From a numerical viewpoint, the stronger one wishes to enforce the DMP the more ill behaved the nonlinear discrete equations become. We have thus derived various approximate forms of the new crosswind diffusion operator suitable for numerical implementation. Numerical results on linear test problems have shown that the new approximate operators offer a quite competitive compromise between solution quality and computational cost with respect to existing methods. Finally, we have applied the new crosswind diffusion operator to a strongly nonlinear case: the computation of a Bunsen flame. In this case the DMP was still satisfied both in domains where oscillations were due to dominating convection and in domains where the reaction terms caused numerical oscillations.

Acknowledgment. The authors are thankful to V. Giovangigli for stimulating discussions. The first author gratefully acknowledges funding from the Swedish Foundation for International Cooperation in Research and Higher Education and from the Fonds National Suisse.

References

[1] C. Johnson, U. Nävert, J. Pitkäranta, Finite element methods for linear hyperbolic equations, Comput. Methods Appl. Mech. Engrg. 45 (1984) 285–312.

[2] A. Mizukami, T. Hughes, A Petrov-Galerkin finite element method for convection dominated flows: an accurate upwinding technique for satisfying the maximum principle, Comput. Methods Appl. Mech. Engrg. 50 (1985) 181–193.

[3] T. Hughes, M. Mallet, A. Mizukami, A new finite element formulation for computational fluid dynamics: II. Beyond SUPG, Comput. Methods Appl. Mech. Engrg. 54 (1986) 341–355.

[4] C. Johnson, A. Schatz, L. Wahlbin, Crosswind smear and pointwise error in streamline diffusion finite element methods, Math. Comp. 49 (1987) 25–38.

[5] P. Ciarlet, P.-A. Raviart, Maximum principle and uniform convergence for the finite element method, Comput. Methods Appl. Mech. Engrg. 2 (1973) 17–31.

[6] L. Wahlbin, Maximum norm error estimates in the finite element method with isoparametric quadratic elements and numerical analysis, RAIRON Anal. Numer. 12 (1978) 173–262.

[7] Y. Shih, H. Elman, Modified streamline diffusion schemes for convection-diffusion problems, Comput. Methods Appl. Mech. Engrg. 174 (1999) 137–151.

[8] D. Gilbarg, N. Trudinger, Elliptic Partial Differential Equations of Second Order, 2nd Edition, no. 224 in Comprehensive Studies in Mathematics, Springer-Verlag, Berlin-New York, 1998, revised third printing.

[9] T. Tezduyar, Y. Park, Discontinuity-capturing finite element formulations for nonlinear convection-diffusion-reaction equations, Comput. Methods Appl. Mech. Engrg. 59 (1986) 307–325.

[10] R. Codina, A discontinuity-capturing crosswind dissipation for the finite element solution of the convection-diffusion equation, Comput. Methods Appl. Mech. Engrg. 110 (1993) 325–342.

[11] S. Idelsohn, N. Nigro, M. Storti, G. Buscaglia, A Petrov-Galerkin formulation for advection-reaction-diffusion problems, Comput. Methods Appl. Mech. Engrg. 136 (1996) 27–46.

[12] T. Ikeda, Maximum principle in finite element models for convection-diffusion phenomena, Vol. 4 of Lecture Notes in Numerical and Applied Analysis, North Holland/Kinokuniya, 1983.

[13] R. LeVeque, Numerical Methods for Conservation Laws, Birkhäuser, Basel, 1990.

[14] G. Strang, G. Fix, An Analysis of the Finite Element Method, Prentice Hall, Englewood Cliffs, N.J., 1973.

[15] S. Korotov, M. Křížek, P. Neittaanmäki, Weakened acute type condition for tetrahedral triangulations and the discrete maximum principle, Math. Comp. 70 (233) (2000) 107–119.

[16] C. Johnson, Numerical Solution of Partial Differential Equations by the Finite Element Method, Cambridge University Press, Cambridge, 1987.

[17] G. Lube, An asymptotically fitted finite element method for convection dominated convection-diffusion-reaction problems, Math. Mech. 72 (1992) 189–200.

[18] S. Rebay, Efficient unstructured mesh generation by means of Delaunay triangulation and Bowyer-Watson algorithm, J. Comput. Phys. 106 (1993) 125–138.

[19] A. Ern, V. Giovangigli, Thermal diffusion effects in hydrogen-air and methane-air flames, Combust. Theory Modelling 2 (1998) 349–372.